Vibronic coupling in benzene cation and anion: Vibronic coupling and frontier electron density in Jahn-Teller molecules

AUTHOR(S):

Tokunaga, Ken; Sato, Tohru; Tanaka, Kazuyoshi

CITATION:

Tokunaga, Ken ...[et al]. Vibronic coupling in benzene cation and anion: Vibronic coupling and frontier electron density in Jahn-Teller molecules. The Journal of Chemical Physics 2006, 124(15): 154303.

ISSUE DATE:

2006-04-21

URL:

http://hdl.handle.net/2433/50523

THE JOURNAL OF CHEMICAL PHYSICS **124**, 154303 (2006)

Vibronic coupling in benzene cation and anion: Vibronic coupling and frontier electron density in Jahn-Teller molecules

Ken Tokunaga
Department of Molecular Engineering, School of Engineering, Kyoto University, Kyoto 615-8510, Japan

Tohru Sato[a)]
Department of Molecular Engineering, School of Engineering, Kyoto University, Kyoto 615-8510, Japan and Fukui Institute for Fundamental Chemistry, Kyoto University, Takano-Nishihiraki-cho 34-4, Sakyo-ku, Kyoto 606-8103, Japan

Kazuyoshi Tanaka
Department of Molecular Engineering, School of Engineering, Kyoto University, Kyoto 615-8510, Japan and Core Research for Evolutional Science and Technology, Japan Science and Technology Agency (JST-CREST)

(Received 25 January 2006; accepted 13 February 2006; published online 17 April 2006)

Vibronic coupling constants of Jahn-Teller molecules, benzene radical cation and anion, are computed as matrix elements of the electronic part of the vibronic coupling operator using the electronic wave functions calculated by generalized restricted Hartree-Fock and state-averaged complete active space self-consistent-field methods. The calculated vibronic coupling constants for benzene cation agree well with the experimental and theoretical values. Vibronic coupling density analysis, which illustrates the local properties of the coupling, is performed in order to explain the order of magnitude of the coupling constant from view of the electronic and vibrational structures. This analysis reveals that the couplings of the $e_{2g}(2)$ and $e_{2g}(3)$ modes in which the large displacements locate on C–C bonds are strong in the cation. On the other hand, they are greatly weakened in the anion because of the decrease of electron density in the region of the C–C bonds, which originates from the antibonding nature of the singly occupied molecular orbital of the anion. However, the difference of the electronic structure has a little influence on the vibronic coupling of the $e_{2g}(4)$ mode. These results indicate that the vibronic coupling depends not only on the direction of the nuclear displacement but also on the frontier electron density. © *2006 American Institute of Physics*. [DOI: 10.1063/1.2184317]

I. INTRODUCTION

Vibronic interaction or electron-vibration (phonon) interaction is one of the most investigated problems in molecular physics[1–4] since it plays an important role not only in solid state physics but also in chemical reaction theory, for instance, Jahn-Teller (JT) effect,[5] superconductivity, electron transfer reaction, and so on. Therefore, vibronic coupling constant (VCC) which rules the magnitude of the interaction has been calculated by many researchers.

For benzene cation, Johnson[6] has obtained VCC by the quadratic fit to the adiabatic potential energy curve. Döscher *et al.*[7] have calculated the derivative of the adiabatic potential energy at the Jahn-Teller origin $\boldsymbol{R}_0$ (see Fig. 1). Applegate and Miller[8] calculated from the distortion vector. In the degenerate electronic state, symmetry breaking[9] in the electronic wave function, which makes the coupling matrix symmetry broken, is inevitable unless the state-averaged calculation is employed. In our previous work,[10] this has been resolved by calculating the vibronic coupling integrals as matrix elements of the electronic part of vibronic coupling operator over wave functions obtained by state-averaged calculation. Furthermore, we have proposed a concept of *vibronic coupling density* which illustrates the local property of vibronic coupling. An analysis with the vibronic coupling density was found to be useful in order to elucidate the magnitude of the interaction.

In the present work, we focus on the vibronic coupling of Jahn-Teller molecules, $C_6H_6^+(Bz^+)$ and $C_6H_6^-(Bz^-)$, in their electronic ground states, $^2E_{1g}$ and $^2E_{2u}$, respectively. (see Figs. 2 and 3). Bz^+ has long been a textbook example for various aspects of vibronic coupling, both in experiment[11–13] and in theory.[14–18] Recent high-resolutional techniques such as mass-analyzed threshold ionization spectroscopy (MATI),[19] zero electron kinetic energy spectroscopy (ZEKE),[20] and photoinduced Rydberg ionization (PIRI) spectroscopy[21] have shed light on the vibronic structure of Bz^+ with the help of the theoretical calculation.[7,8,22–26] Though Bz^- has also been an example of Jahn-Teller effect in experiment[15,27–29] and theory,[30–32] vibronic structure has not been observed. Since the vibrational structures of Bz^+ and Bz^- could be almost the same, comparing their VCCs we can discuss the effect of their electronic structures on the coupling.

Since the electronic ground states of Bz^+ and Bz^- with D_{6h} symmetry are degenerate, the electronic motion couples

[a)]Electronic mail: tsato@scl.kyoto-u.ac.jp

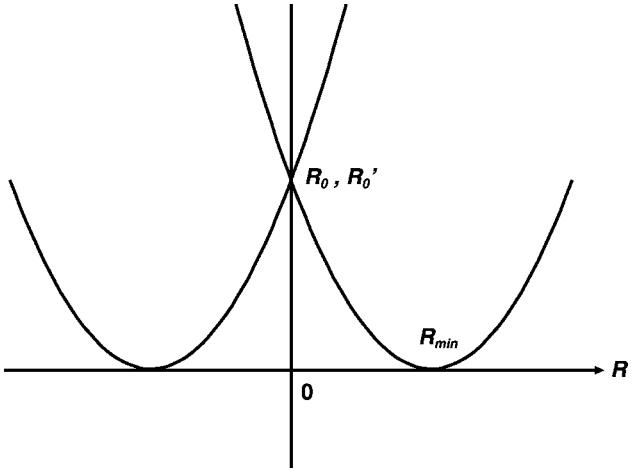

FIG. 1. Cross section of the Jahn-Teller potential. Jahn-Teller crossing $\boldsymbol{R}_0$ is the nuclear configuration of the molecule without Jahn-Teller distortion, and energy minimum $\boldsymbol{R}_{\min}$ is the molecular structure with the lowest energy. The D_{6h} symmetry at $\boldsymbol{R}_0$ is lowered into the D_{2h} at $\boldsymbol{R}_{\min}$ because of the Jahn-Teller effect. For the structure $\boldsymbol{R}_0'$ which is obtained after the conical intersection search, the energy difference $E_e(\boldsymbol{R}_0')-E_e(\boldsymbol{R}_{\min})=\hbar\omega\cdot D^2/2$ is called Jahn-Teller stabilization energy ΔE, where D is dimensionless vibronic coupling constant.

to the vibrational degrees of freedom due to the JT effect. Such JT-active mode is deduced from the symmetric products of electronic states,

$$[E_{1g}^2]=[E_{2u}^2]=a_{1g}\oplus e_{2g}. \tag{1}$$

Among $3N-6=30$ molecular vibrations,

$$\Gamma_{\text{vib}}=2a_{1g}\oplus a_{2g}\oplus 2b_{2g}\oplus e_{1g}\oplus 4e_{2g}\oplus a_{2u}\oplus 2b_{1u}\oplus 2b_{2u}\oplus 3e_{1u}\oplus 2e_{2u}, \tag{2}$$

the vibrational modes which couple to the electronic states are the two a_{1g} and four e_{2g} modes.

VCC of single Slater determinant is equal to the sum of the integrals over molecular orbital which is called orbital vibronic coupling integral (OVCI). The concept of OVCI was first proposed by Bersuker more than two decades ago,[33–35] and has been widely used in solid state and molecular physics. Interesting researches using the OVC have been piled up in many field, for instance, charge transfer reaction,[36] mixed-valence systems,[37] superconductivity,[38] Peierls distortion,[39] and so on.[4] In the case of the coupling between the degenerate electronic state and degenerate modes, VCC is equal to the OVCI over frontier molecular orbital.[10] Thus, VCCs of Bz^+ and Bz^- are equal to OVCIs

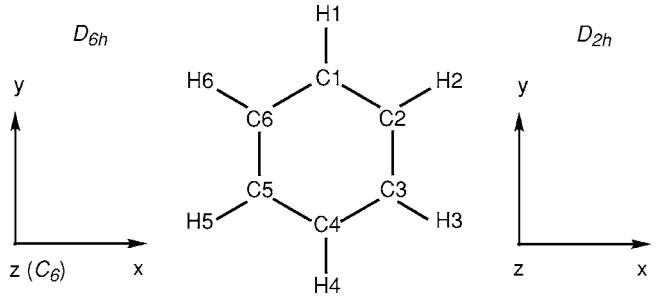

FIG. 2. Structure of benzene and the axes. Because of the Jahn-Teller effect, symmetry of the structure of the cation or anion is lowered from D_{6h} to D_{2h}.

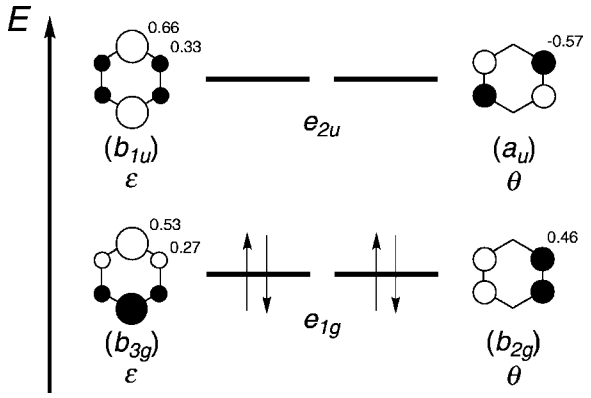

FIG. 3. Frontier π orbitals of benzene obtained by RHF/STO-6G. Inserted values are the molecular coefficients. Because of the sixfold symmetry, the orbital levels of both HOMO and LUMO are doubly degenerate e_{1g} and e_{2u}, respectively. One of doubly degenerate orbitals is denoted as ϵ, and the other θ. Irreducible representations in the parentheses are those lowered into the subgroup D_{2h}; $E_{1g}\downarrow D_{2h}=b_{2g}\oplus b_{3g}$ in HOMO and $E_{1g}\downarrow D_{2h}=a_u\oplus b_{1u}$ in LUMO. ϵ and θ in HOMO are b_{3g} and b_{2g}, respectively, and those in LUMO are b_{1u} and a_u, respectively.

over $\psi_{e_{1g}}\theta$ [highest occupied molecular orbital (HOMO)] and $\psi_{e_{2u}}\theta$ [lowest unoccupied molecular orbital (LUMO)], respectively, as discussed in Sec. III. Hence, VCCs of Bz^+ and Bz^- can directly be affected by the orbital patterns of $\psi_{e_{1g}}\theta$ and $\psi_{e_{2u}}\theta$. Vibronic coupling density analysis will be suitable

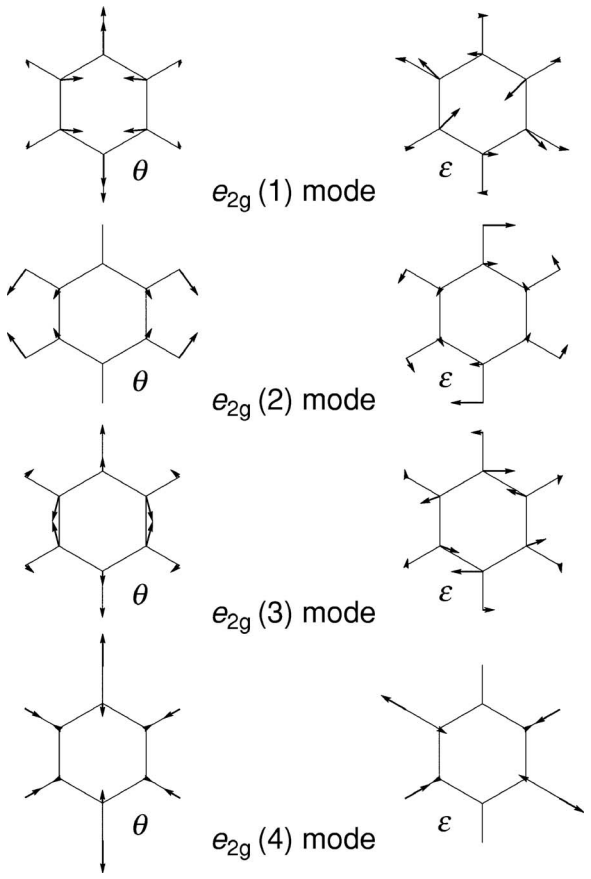

FIG. 4. Jahn-Teller active e_{2g} vibrational modes. The largest displacement locates on the carbon atoms for $e_{2g}(1)$ and $e_{2g}(3)$, and on hydrogen atoms for $e_{2g}(2)$ and $e_{2g}(4)$. The displacements of C2 and H2 atoms (see Fig. 2) in θ modes greatly contribute to the OVCIs, $\langle\psi_{e_{1g}\theta}|v_{e_{2g}\theta}|\psi_{e_{1g}\theta}\rangle$ and $\langle\psi_{e_{2u}\theta}|v_{e_{2g}\theta}|\psi_{e_{2u}\theta}\rangle$.

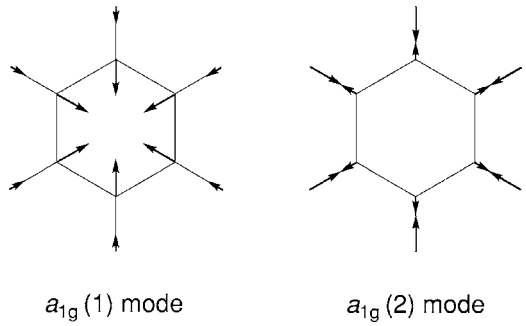

FIG. 5. Totally symmetric a_{1g} vibrational modes. The largest displacement locates on the carbon atoms for $a_{1g}(1)$, and on hydrogen atoms for $a_{1g}(2)$.

for such an analysis because it has the advantage of illustrating the local properties of the vibronic coupling from the electronic structure.

This paper is organized as follows: in Sec. II, we will describe the vibronic Hamiltonian, Sec. III is devoted to the computational details, and Sec. IV deals with the result of calculation using generalized restricted Hartree-Fock (GRHF) and state-averaged complete active space self-consistent-field (CASSCF) wave functions. We will also discuss the relation between the magnitude of vibronic coupling and the orbital patterns of the frontier orbitals with the vibronic coupling density analysis in this section. Finally, we conclude this work in Sec. V.

II. VIBRONIC HAMILTONIAN

The model Hamiltonian employed here is[10]

$$\mathcal{H} = \sum_i -\frac{\hbar^2}{2}\left(\frac{\partial^2}{\partial Q_i^2}\right) + \mathcal{H}_e(\boldsymbol{r},\boldsymbol{R}_0) + \sum_i \left(\frac{\partial \mathcal{U}}{\partial Q_i}\right)_{\boldsymbol{R}_0} Q_i + \sum_i \frac{1}{2}\omega_i^2 Q_i^2, \tag{3}$$

where $\boldsymbol{r}$ is a set of electronic coordinates, Q_i a normal coordinate of the ith mode, $\mathcal{H}_e$ an electronic Hamiltonian, $\mathcal{U}$ a sum of an electron-electron, electron-nuclear, nuclear-nuclear potential operator, and ω_i a frequency of the ith mode. Only the linear vibronic coupling is considered. The operator involved in the third term,

$$\mathcal{V}_i = \left(\frac{\partial \mathcal{U}}{\partial Q_i}\right)_{\boldsymbol{R}_0}, \tag{4}$$

is called the electronic operator of the ith mode, and $Q_i\mathcal{V}_i$ describes the vibronic coupling. We treat the model Hamiltonian within the space spanned by the electronic states $|E\theta\rangle$ and $|E\epsilon\rangle$,

$$\hat{\mathcal{H}}_{\mathrm{JT}} = \left[E_0 + \sum_i \left\{-\frac{\hbar^2}{2}\left(\frac{\partial^2}{\partial Q_i^2}\right) + \frac{1}{2}\omega_i^2 Q_i^2\right\}\right]\hat{\sigma}_0 + \sum_i \begin{pmatrix} \langle E\theta|\mathcal{V}_i|E\theta\rangle & \langle E\theta|\mathcal{V}_i|E\epsilon\rangle \\ \langle E\epsilon|\mathcal{V}_i|E\theta\rangle & \langle E\epsilon|\mathcal{V}_i|E\epsilon\rangle \end{pmatrix} Q_i, \tag{5}$$

where $\{|E\theta\rangle, |E\epsilon\rangle\}$ denotes the degenerate electronic state $\{|E_{1g}\theta\rangle, |E_{1g}\epsilon\rangle\}$ for Bz^+ or $\{|E_{2u}\theta\rangle, |E_{2u}\epsilon\rangle\}$ for Bz^-, E_0 eigenenergy of $\mathcal{H}_e$, and

$$\hat{\sigma}_0 = \begin{pmatrix} 1 & 0 \\ 0 & 1 \end{pmatrix}. \tag{6}$$

The coupling matrix can be reduced using Wigner-Eckart theorem as

$$\hat{V}_{e_{2g}\theta(j)} = \begin{pmatrix} \langle E\theta|\mathcal{V}_{\theta(j)}|E\theta\rangle & \langle E\theta|\mathcal{V}_{\theta(j)}|E\epsilon\rangle \\ \langle E\epsilon|\mathcal{V}_{\theta(j)}|E\theta\rangle & \langle E\epsilon|\mathcal{V}_{\theta(j)}|E\epsilon\rangle \end{pmatrix} = V_{e_{2g}(j)}\begin{pmatrix} 1 & 0 \\ 0 & -1 \end{pmatrix}, \tag{7}$$

and

$$\hat{V}_{e_{2g}\epsilon(j)} = \begin{pmatrix} \langle E\theta|\mathcal{V}_{\epsilon(j)}|E\theta\rangle & \langle E\theta|\mathcal{V}_{\epsilon(j)}|E\epsilon\rangle \\ \langle E\epsilon|\mathcal{V}_{\epsilon(j)}|E\theta\rangle & \langle E\epsilon|\mathcal{V}_{\epsilon(j)}|E\epsilon\rangle \end{pmatrix} = V_{e_{2g}(j)}\begin{pmatrix} 0 & 1 \\ 1 & 0 \end{pmatrix}, \tag{8}$$

where the integrals $\langle E\theta|\mathcal{V}_{\theta(j)}|E\theta\rangle$ and so on are called VCIs. VCC is defined as

$$V_{e_{2g}(j)} = \langle E\theta|\mathcal{V}_{\theta(j)}|E\theta\rangle = -\langle E\epsilon|\mathcal{V}_{\theta(j)}|E\epsilon\rangle = \langle E\theta|\mathcal{V}_{\epsilon(j)}|E\epsilon\rangle = \langle E\epsilon|\mathcal{V}_{\epsilon(j)}|E\theta\rangle,$$

which is the quantity we will calculate in this article. On the

TABLE I. Bond lengths (Å) of neutral benzene calculated using RHF/6−31G(d,p) and that of the radical ions with the D_{6h} symmetry using GRHF/6−31G(d,p). Note that the geometrical structure of neutral benzene is employed throughout this work.

Species	Method	C–C	C–H
Neutral	RHF	1.3859	1.0760
Cation	GRHF	1.3990	1.0742
Anion	GRHF	1.4056	1.0811

TABLE II. Frequencies (cm^{-1}) of neutral benzene calculated using RHF/6−31G(d,p) with the structure optimized by RHF/6−31G(d,p) and that of the radical ions with the D_{6h} symmetry calculated using GRHF/6−31G(d,p) with the structure optimized by GRHF/6−31G(d,p) in each ionic state. Note that there is little difference between RHF and GRHF calculations.

Species	Method	$a_{1g}(1)$	$a_{1g}(2)$	$e_{2g}(1)$	$e_{2g}(2)$	$e_{2g}(3)$	$e_{2g}(4)$
Neutral	RHF	1083	3373	665	1288	1795	3343
Cation	GRHF	1058	3405	645	1297	1776	3388
Anion	GRHF	1043	3302	638	1251	1735	3302

TABLE III. Total energy (a.u.) and vibronic coupling constant V (10^{-4} a.u.) of Bz^+. Basis set employed is 6−31G(d,p). The vibrational vectors employed are those obtained by RHF/6−31G(d,p) for neutral benzene.

Energy	RHF −230.3831[a]	GRHF −230.4084	CAS(3,4) −230.4303	CAS(5,5) −230.4550	CAS(5,6) −230.4779
$a_{1g}(1)$	39.51	64.96	6.67	6.90	7.53
$a_{1g}(2)$	20.63	42.24	2.59	2.52	2.28
$e_{2g}(1)$	−10.29	−10.48	−9.78	−8.62	−7.15
$e_{2g}(2)$	11.95	11.86	11.52	10.21	9.31
$e_{2g}(3)$	17.47	17.09	17.03	15.11	14.31
$e_{2g}(4)$	6.67	6.75	6.58	5.76	4.20

[a]The energy is estimated using Koopmans' theorem. The energy of neutral benzene is −230.7139 a.u. and the orbital energy of HOMO is −0.3307 a.u.

other hand, the interaction matrix between vibrational a_{1g} mode k is written as

$$\hat{V}_{a_{1g}(k)} = \begin{pmatrix} \langle E\theta|\mathcal{V}_{a_{1g}(k)}|E\theta\rangle & \langle E\theta|\mathcal{V}_{a_{1g}(k)}|E\epsilon\rangle \\ \langle E\epsilon|\mathcal{V}_{a_{1g}(k)}|E\theta\rangle & \langle E\epsilon|\mathcal{V}_{a_{1g}(k)}|E\epsilon\rangle \end{pmatrix} = V_{a_{1g}(k)} \begin{pmatrix} 1 & 0 \\ 0 & 1 \end{pmatrix}, \tag{9}$$

where

$$V_{a_{1g}(k)} = \langle E\theta|\mathcal{V}_{a_{1g}(k)}|E\theta\rangle = \langle E\epsilon|\mathcal{V}_{a_{1g}(k)}|E\epsilon\rangle \tag{10}$$

is a VCC for a totally symmetric a_{1g} mode. The VCC can be obtained from a calculation of the VCI.

Finally, we introduce here some dimensionless quantities. For a vibrational mode i, the normal coordinate Q_i is measured by $\sqrt{\hbar/\omega_i}$,

$$Q_i = \sqrt{\frac{\hbar}{\omega_i}} q_i, \tag{11}$$

where q_i is a dimensionless normal coordinate. Dimensionless coupling constant D_i can be defined as

$$D_i = \frac{V_i}{\sqrt{\hbar \omega_i^3}}. \tag{12}$$

III. METHOD OF CALCULATION

As a reference structure $\boldsymbol{R}_0$ of the JT system, we take the structure of neutral benzene, which is called *parent system*

TABLE IV. Total energy (a.u.) and vibronic coupling constant V (10^{-4} a.u.) of Bz^-. Basis set employed is 6−31G(d,p). The vibrational vectors employed are those obtained by RHF/6−31G(d,p) for neutral benzene.

Energy	RHF −230.5648[a]	GRHF −230.5858	CAS(5,4) −230.6052	CAS(7,5) −230.6075	CAS(7,6) −230.6412
$a_{1g}(1)$	−32.51	−7.29	−6.94	−6.86	−5.81
$a_{1g}(2)$	−11.68	9.67	9.58	9.57	9.30
$e_{2g}(1)$	5.85	5.74	5.69	4.54	4.18
$e_{2g}(2)$	1.27	1.24	0.93	2.08	2.19
$e_{2g}(3)$	5.71	5.73	5.17	6.75	6.79
$e_{2g}(4)$	−7.84	−7.98	−7.89	−7.11	−6.76

[a]The energy is estimated using Koopmans' theorem. The energy of neutral benzene is −230.7139 a.u. and the orbital energy of LUMO is 0.1491 a.u.

TABLE V. Unscaled dimensionless vibronic coupling constants D of Bz^+. The vibrational vectors and frequencies employed in these calculations were obtained with RHF/6−31G(d,p) for neutral benzene. Negative signs are neglected.

	RHF	GRHF	CAS(3,4)	CAS(5,5)	CAS(5,6)
$a_{1g}(1)$	11.39	18.73	1.92	1.99	2.17
$a_{1g}(2)$	1.08	2.22	0.14	0.13	0.12
$e_{2g}(1)$	6.17	6.28	5.86	5.17	4.29
$e_{2g}(2)$	2.66	2.64	2.56	2.27	2.07
$e_{2g}(3)$	2.36	2.31	2.30	2.04	1.93
$e_{2g}(4)$	0.35	0.36	0.35	0.31	0.22

throughout this article. Since the parent system does not give rise to any JT distortion, its geometry has D_{6h} symmetry.

The electronic operator $\mathcal{V}_i$ is a sum of one-electron operators $v_i(a)$ and the derivative of the nuclear-nuclear repulsion potential $\mathcal{U}_{\rm nn}$ with respect to Q_i,

$$\mathcal{V}_i = -\sum_a \sum_\alpha \left[\frac{\partial}{\partial Q_i} \left(\frac{Z_\alpha e^2}{|\boldsymbol{r}_a - \boldsymbol{R}_\alpha|} \right) \right]_{\boldsymbol{R}_0} + \frac{\partial \mathcal{U}_{\rm nn}}{\partial Q_i} = \sum_a v_i(a) + \frac{\partial \mathcal{U}_{\rm nn}}{\partial Q_i}, \tag{13}$$

where indices α and a denote nucleus and electron and Z_α charge of the nucleus α. It should be noted that $\partial \mathcal{U}_{\rm nn}/\partial Q_i$ is zero except for the a_{1g} modes.

For the HF methods, the wave functions for E states are written as a single Slater determinant,

$$|E_{1g}\theta(\mathrm{HF})\rangle = |\cdots \psi_m \alpha \psi_m \beta \cdots \psi_{e_{1g}\theta} \alpha \psi_{e_{1g}\epsilon} \alpha \psi_{e_{1g}\epsilon} \beta\rangle =: |\theta\rangle, \tag{14}$$

TABLE VI. Dimensionless scaled vibronic coupling constants D' of Bz^+ calculated by CASSCF(5,6)/6−31G(d,p) for Bz^+. Negative signs are neglected.

Method	$e_{2g}(1)$	$e_{2g}(2)$	$e_{2g}(3)$	$e_{2g}(4)$
Present work	1.15	0.56	0.52	0.06
Calc. (Ref. 16[a])	1.666	0.373	1.240	0.031
Calc. (Ref. 17[a])	1.313	0.680	1.134	0.0
Calc. (Ref. 42[a])	0.95	0.49	0.76	0.1
Calc. (Ref. 7[b])	0.983	0.510	0.800	0.008
Calc. (Ref. 7[b])	0.997	0.529	0.742	0.011
Calc. (Ref. 8[c])	0.92	0.49	0.68	<0.14
Calc. (Ref. 6[d])	0.98	0.45	0.77	
Expt. (Ref. 22)	1.0			
Expt. (Ref. 24)	0.88			
Expt. (Ref. 25)	0.868			
Expt. (Refs. 8 and 24)	1.01	0.49	0.60	
Expt. (Ref. 26)	1.02	0.49	0.62	

[a]VCC is calculated from derivative of one-electron orbital energy at $\boldsymbol{R}_0$.
[b]VCC is calculated from derivative of the adiabatic potential energy at $\boldsymbol{R}_0$.
[c]VCC is calculated from distortion vector.
[d]VCC is calculated from quadratic fit to the adiabatic potential.

TABLE VII. Unscaled dimensionless vibronic coupling constants D of Bz^-. The vibrational vectors and frequencies employed in these calculations were obtained with RHF/6−31G(d,p) for neutral benzene. Negative signs are neglected.

	RHF	GRHF	CAS(5,4)	CAS(7,5)	CAS(7,6)
$a_{1g}(1)$	9.38	2.10	2.00	1.98	1.68
$a_{1g}(2)$	0.61	0.51	0.50	0.50	0.49
$e_{2g}(1)$	3.51	3.44	3.41	2.72	2.51
$e_{2g}(2)$	0.28	0.27	0.21	0.46	0.49
$e_{2g}(3)$	0.77	0.77	0.70	0.91	0.92
$e_{2g}(4)$	0.42	0.42	0.42	0.38	0.36

$$|E_{1g}\epsilon(\mathrm{HF})\rangle = |\cdots\psi_m\alpha\psi_m\beta\cdots\psi_{e_{1g}\theta}\alpha\psi_{e_{1g}\epsilon}\alpha\psi_{e_{1g}\theta}\beta\rangle =: |\epsilon\rangle, \tag{15}$$

for Bz^+, and

$$|E_{2u}\theta(\mathrm{HF})\rangle = |\cdots\psi_m\alpha\psi_m\beta\cdots\psi_{e_{2u}\theta}\alpha\rangle =: |\theta\rangle, \tag{16}$$

$$|E_{2u}\epsilon(\mathrm{HF})\rangle = |\cdots\psi_m\alpha\psi_m\beta\cdots\psi_{e_{2u}\epsilon}\alpha\rangle =: |\epsilon\rangle, \tag{17}$$

for Bz^-, and α, β are spin functions.

The vibronic coupling matrix for the HF wave function is given by

$$\hat{V}_i^{\mathrm{HF}} = \begin{pmatrix} \langle\theta|\mathcal{V}_i|\theta\rangle & \langle\theta|\mathcal{V}_i|\epsilon\rangle \\ \langle\epsilon|\mathcal{V}_i|\theta\rangle & \langle\epsilon|\mathcal{V}_i|\epsilon\rangle \end{pmatrix}. \tag{18}$$

For the e_{2g} modes, the VCI over Slater determinants $|\theta\rangle$ and $|\epsilon\rangle$ can be decomposed into OVCIs for the θ mode over molecular orbitals,

$$\begin{aligned} V_{e_{2g}(j)} &= \langle\theta|\mathcal{V}_\theta|\theta\rangle = -\langle\epsilon|\mathcal{V}_\theta|\epsilon\rangle \\ &= \sum_{m\in E_{1g}\oplus E_{2g}\oplus E_{1u}\oplus E_{2u}} \{n_{\theta(m)}\langle\psi_{\theta(m)}|v_\theta|\psi_{\theta(m)}\rangle \\ &\quad + n_{\epsilon(m)}\langle\psi_{\epsilon(m)}|v_\theta|\psi_{\epsilon(m)}\rangle\}, \end{aligned} \tag{19}$$

where m runs over the occupied molecular orbitals with E_{1g}, E_{2g}, E_{1u}, and E_{2u} symmetries, and $\psi_{\theta(m)}$ and $\psi_{\epsilon(m)}$ denote the degenerate pair of molecular orbitals. $n_{\theta(m)}$ and $n_{\theta(m)}$ are occupation numbers of $\psi_{\theta(m)}$ and $\psi_{\epsilon(m)}$. Note that the orbitals with the E_{1g}, E_{2g}, E_{1u}, and E_{2u} symmetries can couple to the e_{2g} modes since $[E_{1g}^2]=[E_{2g}^2]=[E_{1u}^2]=[E_{2u}^2]=A_{1g}\oplus E_{2g}$. Furthermore, it should be noted here that

$$\langle\psi_{\theta(m)}|v_\theta|\psi_{\theta(m)}\rangle + \langle\psi_{\epsilon(m)}|v_\theta|\psi_{\epsilon(m)}\rangle = 0. \tag{20}$$

Therefore, the vibronic coupling matrix in the HF methods is equal to the OVCI matrix,

TABLE VIII. Dimensionless scaled vibronic coupling constants D' of Bz^- calculated by CASSCF(7,6)/6−31G(d,p). Negative signs are neglected.

Method	$e_{2g}(1)$	$e_{2g}(2)$	$e_{2g}(3)$	$e_{2g}(4)$
Present work	1.43	0.28	0.52	0.21
Calc. (Ref. 16[a])	0.870	0.528	1.09	0.096
Calc. (Ref. 17[a])	0.33	0.759	1.28	0.1
Calc. (Ref. 42[a])	0.42	0.61	0.97	0.1

[a]VCC is calculated from the derivative of one-electron orbital energy at $\boldsymbol{R}_0$.

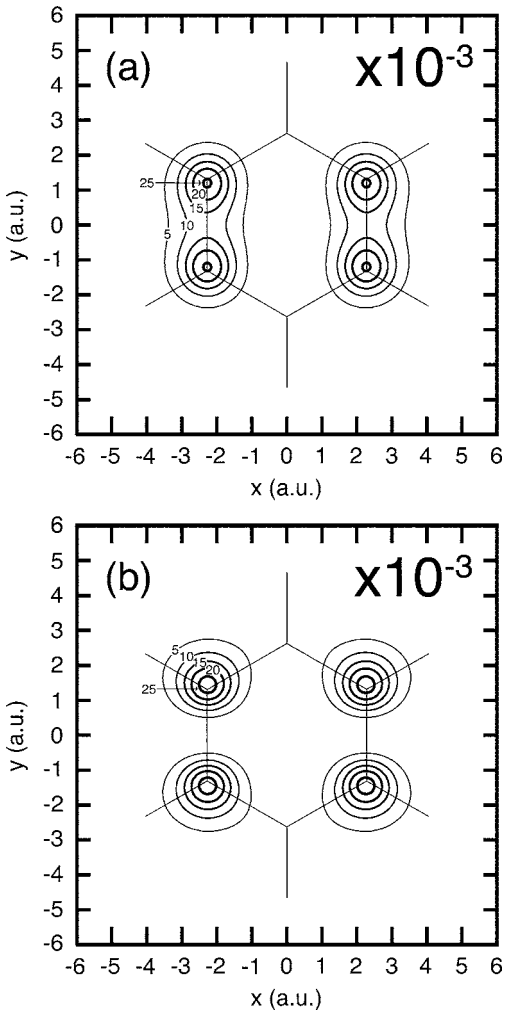

FIG. 6. Contour plot of the electron density $\rho_\theta(\boldsymbol{r})$ for (a) $\psi_{e_{1g}\theta}$ (HOMO) and (b) $\psi_{e_{2u}\theta}$ (LUMO) calculated by the GRHF/6-31G(d,p) method on the plane z=1.0.

$$\hat{V}_\theta^{\mathrm{HF}} = \begin{pmatrix} \langle\psi_{e_{1g}\epsilon}|v_\theta|\psi_{e_{1g}\epsilon}\rangle & 0 \\ 0 & \langle\psi_{e_{1g}\theta}|v_\theta|\psi_{e_{1g}\theta}\rangle \end{pmatrix}, \tag{21}$$

$$\hat{V}_\epsilon^{\mathrm{HF}} = \begin{pmatrix} 0 & \langle\psi_{e_{1g}\epsilon}|v_\epsilon|\psi_{e_{1g}\theta}\rangle \\ \langle\psi_{e_{1g}\theta}|v_\epsilon|\psi_{e_{1g}\epsilon}\rangle & 0 \end{pmatrix}, \tag{22}$$

for Bz^+, and

$$\hat{V}_\theta^{\mathrm{HF}} = \begin{pmatrix} \langle\psi_{e_{2u}\theta}|v_\theta|\psi_{e_{2u}\theta}\rangle & 0 \\ 0 & \langle\psi_{e_{2u}\epsilon}|v_\theta|\psi_{e_{2u}\epsilon}\rangle \end{pmatrix}, \tag{23}$$

$$\hat{V}_\epsilon^{\mathrm{HF}} = \begin{pmatrix} 0 & \langle\psi_{e_{2u}\theta}|v_\epsilon|\psi_{e_{2u}\epsilon}\rangle \\ \langle\psi_{e_{2u}\epsilon}|v_\epsilon|\psi_{e_{2u}\theta}\rangle & 0 \end{pmatrix}, \tag{24}$$

for Bz^-.

As for the a_{1g} modes, there is no such cancellation,

$$V_{a_{1g}(k)} = \langle\theta|\mathcal{V}_{a_{1g}(k)}|\theta\rangle = \langle\epsilon|\mathcal{V}_{a_{1g}(k)}|\epsilon\rangle = \sum_m \langle\chi_m|v_{a_{1g}(k)}|\chi_m\rangle + \frac{\partial\mathcal{U}_{\mathrm{nn}}}{\partial Q_{a_{1g}(k)}} = \sum_{m'} \langle\chi_{m'}|v_{a_{1g}(k)}|\chi_{m'}\rangle + \frac{\partial\mathcal{U}_{\mathrm{nn}}}{\partial Q_{a_{1g}(k)}}, \quad (25)$$

where m and m' run over the occupied spin orbitals of $|\theta\rangle$ and $|\epsilon\rangle$, respectively.

Here, we define the scaled dimensionless vibronic coupling constant D',

$$D' = \kappa D, \quad (26)$$

where κ is a scaling parameter which satisfies the relation,

$$\Delta E = \sum_{j=1}^{4} \hbar\omega_j \frac{D_j'^2}{2} = \kappa^2 \sum_{j=1}^{4} \hbar\omega_j \frac{D_j^2}{2}, \quad (27)$$

where ΔE is the energy difference between the minimum structure of the radical optimized within D_{2h} symmetry and the structure of the conical intersection optimized within D_{6h} symmetry. Therefore, D_j' can be calculated from V_j, ω_j, and ΔE.

In order to obtain the optimized geometry $\boldsymbol{R}_0$ and vibrational structure of the parent system, RHF method is employed for the parent system, neutral benzene. At the geometry $\boldsymbol{R}_0$, we employed state-averaged CASSCF method using GAUSSIAN 03 (Ref. 40) and GRHF method using CADPAC (Ref. 41) to determine the wave functions of Bz^+ and Bz^-. All calculations were performed using the 6-31G(d,p) basis set. The VCI was evaluated using these wave functions.

In the vibrational analysis, positive directions of the normal coordinates are defined in Figs. 4 and 5. All quantities are given in a.u. except for bond lengths and wave numbers throughout this article.

IV. RESULTS AND DISCUSSION

A. Geometrical and vibrational structures

The optimized symmetries of the parent system C_6H_6 and that of the conical intersection for the radical ions are D_{6h}. In Table I, the bond lengths of the neutral benzene and the radical ions with the D_{6h} symmetry are tabulated. It is found that the optimized geometries of the energy minimum for benzene and the conical intersection for the radical ions are almost the same. The bond lengths differ within 0.02 Å for C–C and 0.01 Å for the C–H bonds. Thus we take the geometry of neutral benzene as that of the JT crossing point of radical ions in order to save computational resources.

Vibrational frequencies are summarized in Table II. Vibrational structures are also the same. Therefore, we took the geometrical and vibrational structures of neutral benzene as those of the JT crossing structure of the radical ions throughout this study.

B. Vibronic coupling constant

The calculated VCCs of Bz^+ and Bz^- using RHF, GRHF, and CASSCF methods are tabulated in Tables III and IV, respectively. We confirmed that these methods yielded appropriate wave functions with the correct symmetry.[10] Note that the RHF wave function is not variationally optimized for the radicals since the RHF calculation was performed for the parent system, neutral benzene. For the a_{1g} modes, the RHF wave function yields quite large value, comparing with the variationally optimized wave functions. This is because all the occupied orbitals contribute to the VCCs of the a_{1g} modes, and the errors are accumulated, while only frontier e_{1g} or e_{2u} orbitals contribute to those of e_{2g} modes.

1. Benzene cation

In all the calculations of V for Bz^+ shown in Table III, it is found that the order of the coupling is $e_{2g}(3) > e_{2g}(2) > e_{2g}(1) > e_{2g}(4)$, and this agrees with the experimental result. In other words, as long as we are interested in a qualitative aspect of the e_{2g} modes, we can employ the RHF wave function for the VCC calculation.

The calculated D and D' are tabulated in Tables V and VI, respectively. Table VI demonstrates good agreement of the present results with the calculation and experiment except for the fact that the order of $e_{2g}(2)$ and $e_{2g}(3)$ is interchanged.

2. Benzene anion

In all the calculations for Bz^- shown in Table IV, V of the $e_{2g}(2)$ mode has the smallest value among the four e_{2g} modes. The calculated VCCs of Bz^- become smaller, compared with those of Bz^+, and the order of VCCs of $e_{2g}(1)$, $e_{2g}(3)$, and $e_{2g}(4)$ depends on the method of calculation.

The calculated D and D' are tabulated in Tables VII and VIII, respectively. $e_{2g}(1)$ mode has the largest value and $e_{2g}(4)$ has the smallest. This result is the same as Bz^+. Our result agrees with all previous works in the point that $e_{2g}(4)$ has the smallest values and the result of Lipari *et al.*[16] in the point that the $e_{2g}(1)$ has larger coupling than $e_{2g}(2)$.

C. Vibronic coupling density analysis

1. Vibronic coupling density

Vibronic coupling density $\eta_j(\boldsymbol{r})$ (Ref. 10) for the $e_{2g}(j)$ mode is defined by

$$\eta_j(\boldsymbol{r}) = \psi_\theta^*(\boldsymbol{r})\psi_\theta(\boldsymbol{r})v_{\theta(j)}(\boldsymbol{r}) = \rho_\theta(\boldsymbol{r})v_{\theta(j)}(\boldsymbol{r}), \quad (28)$$

where $\rho_\theta(\boldsymbol{r})$ is the frontier electron density of the molecular orbital ψ_θ, and $v_{\theta(j)}(\boldsymbol{r})$ the one-electron operator defined in Eq. (13), $\psi_\theta = \psi_{e_{1g}\theta}$ for Bz^+, and $\psi_\theta = \psi_{e_{2u}\theta}$ for Bz^-. Using η_j, the VCC is written as

$$V_j = \int d\boldsymbol{r}\,\eta_j(\boldsymbol{r}). \quad (29)$$

The vibronic coupling density enables us to analyze the calculated VCC in terms of the electronic structure $\rho_\theta(\boldsymbol{r})$ and the derivative of the potential with respect to the normal coordinate $v_{\theta(j)}(\boldsymbol{r})$.

In Fig. 4, the JT-active e_{2g} modes are shown. It should be noted that the larger components of the vibrational modes lie on the carbon atoms for $e_{2g}(1)$ and $e_{2g}(3)$, while the hydrogen atoms in $e_{2g}(2)$ or $e_{2g}(4)$ have large contribution.

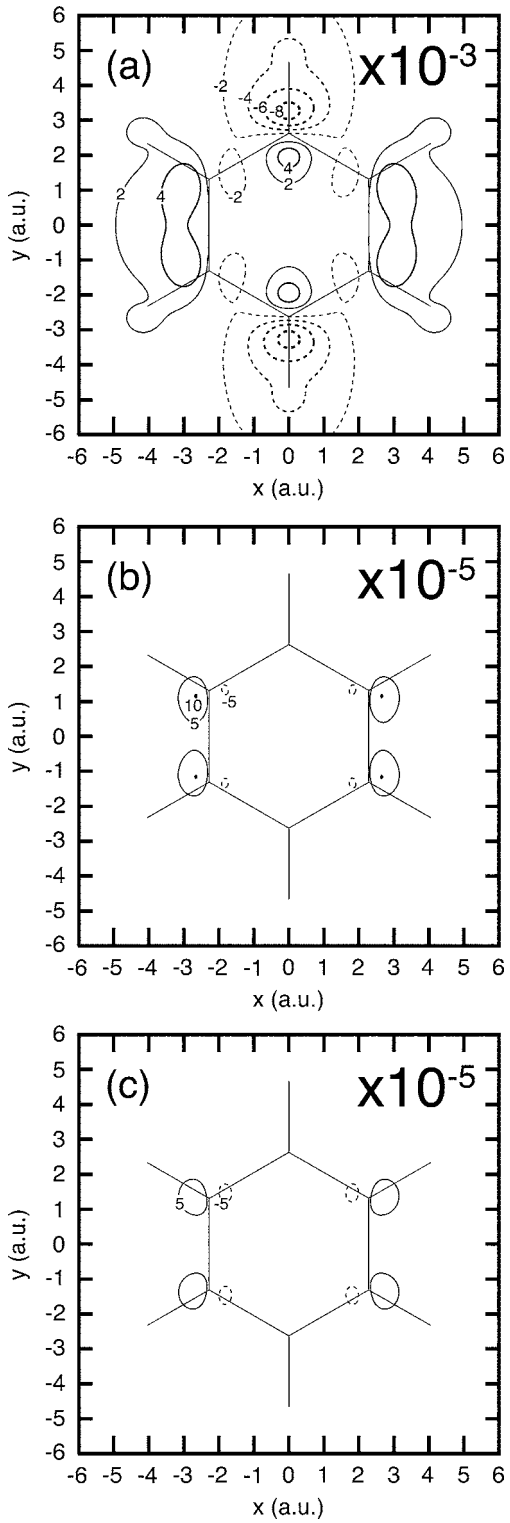

FIG. 7. (a) Contour map of the one-electron vibronic coupling operator $v_\theta(\boldsymbol{r})$ with respect to the $e_{2g}(1)\theta$ mode on the plane $z=1.0$ a.u. (b) Contour map of the vibronic coupling density $\eta_{e_{2g}(1)\theta}(\boldsymbol{r})$ for Bz^+ on the plane $z=1.0$ a.u. (c) Contour map of the vibronic coupling density $\eta_{e_{2g}(1)\theta}(\boldsymbol{r})$ for Bz^- on the plane $z=1.0$ a.u.

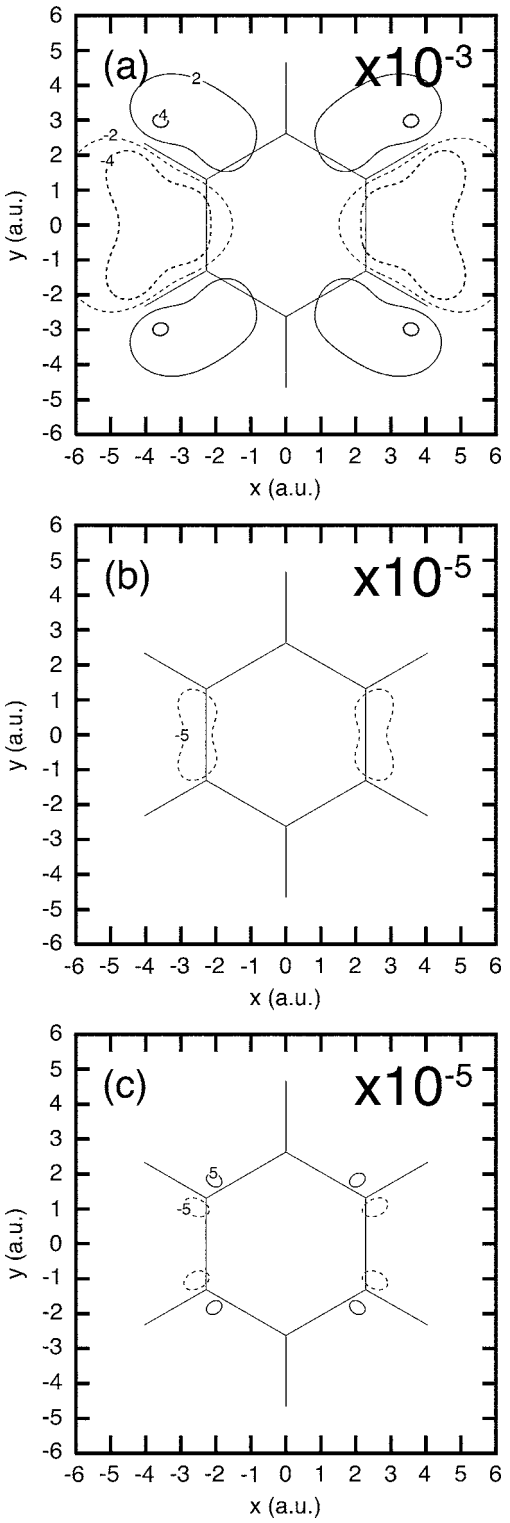

FIG. 8. (a) Contour map of the one-electron vibronic coupling operator $v_\theta(\boldsymbol{r})$ with respect to the $e_{2g}(2)\theta$ mode on the plane $z=1.0$ a.u. (b) Contour map of the vibronic coupling density $\eta_{e_{2g}(2)\theta}(\boldsymbol{r})$ for Bz^+ on the plane $z=1.0$ a.u. (c) Contour map of the vibronic coupling density $\eta_{e_{2g}(2)\theta}(\boldsymbol{r})$ for Bz^- on the plane $z=1.0$ a.u.

2. Benzene cation

Figure 6(a) shows the contour plot of the electron density $\rho_\theta(\boldsymbol{r})$ of $e_{1g}\theta$ orbital calculated from the GRHF wave function.

In Fig. 7(a), the derivative of the potential with respect to the $e_{2g}(1)\theta$ mode is shown. It is found that the large values are distributed around C1 and C4 atoms (see Fig. 2), because the large displacement lies on these atoms. However, there is little electron density around these atoms. Consequently, the vibronic coupling density of this mode η_1 is not so large, as shown in Fig. 7(b).

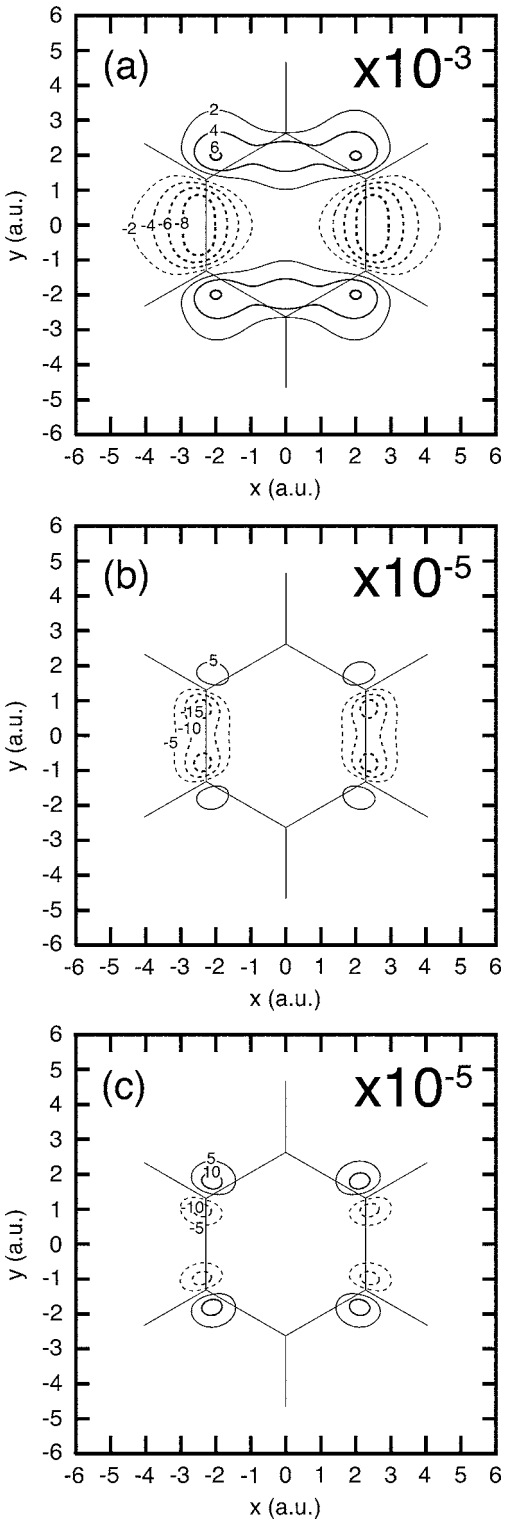

FIG. 9. (a) Contour map of the one-electron vibronic coupling operator $v_\theta(\boldsymbol{r})$ with respect to the $e_{2g}(3)\theta$ mode on the plane $z=1.0$ a.u. (b) Contour map of the vibronic coupling density $\eta_{e_{2g}(3)\theta}(\boldsymbol{r})$ for Bz^+ on the plane $z=1.0$ a.u. (c) Contour map of the vibronic coupling density $\eta_{e_{2g}(3)\theta}(\boldsymbol{r})$ for Bz^- on the plane $z=1.0$ a.u.

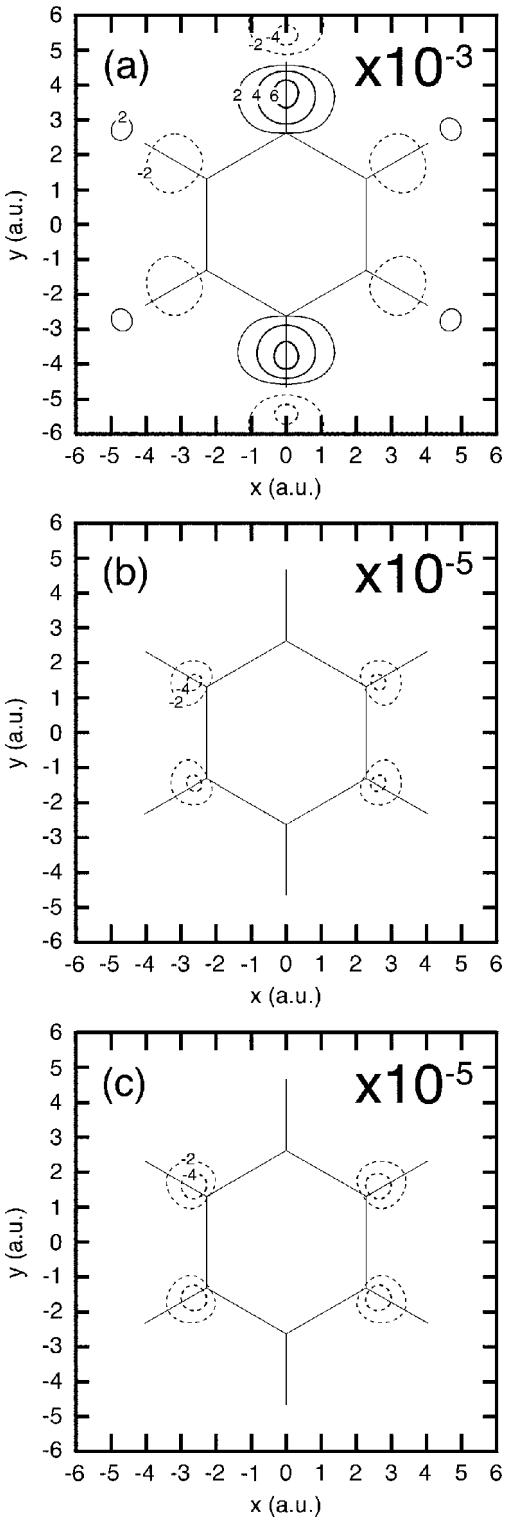

FIG. 10. (a) Contour map $z=1.0$ of the one-electron vibronic coupling operator $v_\theta(\boldsymbol{r})$ with respect to the $e_{2g}(4)\theta$ mode on the plane $z=1.0$ a.u. (b) Contour map of the vibronic coupling density $\eta_{e_{2g}(4)\theta}(\boldsymbol{r})$ for Bz^+ on the plane $z=1.0$ a.u. (c) Contour map of the vibronic coupling density $\eta_{e_{2g}(4)\theta}(\boldsymbol{r})$ for Bz^- on the plane $z=1.0$ a.u.

Figure 8(a) shows the derivative of the potential with respect to the $e_{2g}(2)\theta$ mode. The derivative of the potential has a large value in the region surrounded by H2–C2–C3–H3 and H6–C6–C5–H5. This is because the large displacement of this mode lies on the hydrogen atoms. Since the electron density is localized on the C2–C3 and C5–C6 bonds, the vibronic coupling density for this mode η_2 gives rather large near the C2–C3 and C5–C6 bonds, as shown in Fig. 8(b).

The derivative of the potential with respect to the $e_{2g}(3)\theta$ mode is shown in Fig. 9(a). This mode yields the largest VCC among the four. The derivative plot shows a distribution on the C2–C3 and C5–C6 bonds. Figure 9(b)

shows the vibronic coupling density η_3. As the result of the electron and derivative potential distributions, η_3 is distributed on the C2–C3 and C5–C6 bonds. The broad distribution makes the VCC of this mode large. The coincidence between the electron density distribution ρ_θ and the distribution of the derivative potential v_θ is the reason why the VCC of the $e_{2g}(3)\theta$ mode is the largest among the four.

Figure 10(a) shows the derivative of the potential with respect to the $e_{2g}(4)\theta$ mode. The derivative of the potential has a large value on the area near H1 and H4 atoms. This is because the large displacement of this mode lies on these atoms. The vibronic coupling density of $e_{2g}(4)\theta$ mode [Fig. 10(b)] illustrates low density near H1 and H4 atoms. The distribution of the derivative potential does not coincide with the electron density distribution ρ_θ. This is the reason why the VCC of this mode is the smallest.

It is interesting to note that it is not necessary for the VCC of the mode which has large component on the carbons to be large. In other words, the direction of the nuclear displacement plays an essential role.

3. Benzene anion

Figure 6(b) shows the contour plot of the electron density $\rho_\theta(\boldsymbol{r})$ of the $e_{2u}\theta$ orbital calculated from the GRHF wave function.

Figures 8(c) and 9(c) show the vibronic coupling densities of $e_{2g}(2)\theta$ and $e_{2g}(3)\theta$ modes, respectively. Large reduction of the electron density in the region of C2–C3 and C5–C6 bonds leads to the reduction of the vibronic coupling density in this region. Thus, VCCs of Bz^- of these modes are decreased, compared with those of Bz^+.

Figures 7(c) and 10(c) show the vibronic coupling densities of $e_{2g}(1)\theta$ and $e_{2g}(4)\theta$ modes, respectively. Since these modes have large potential derivative near the midpoint of C–H bonds, large reduction of the electron density on C–C bonds has little effect on the vibronic coupling density. Thus, VCCs of Bz^- of these modes are as large as those of Bz^+.

It is interesting to note that the interactions of $e_{2g}(2)$ and $e_{2g}(3)$ are larger in $Bz^+(\psi_{e_{1g}\theta})$ than $Bz^-(\psi_{e_{2u}\theta})$, but that of $e_{2g}(4)$ are larger in Bz^+. This indicates that the magnitude of the vibronic coupling depends not only on the direction of the nuclear displacement but also on the phase pattern of the orbital.

V. CONCLUSION

We calculate vibronic coupling constants of benzene radical cation and anion. The couplings are computed as matrix elements of the electronic part of the vibronic coupling operator, employing GRHF and state-averaged CASSCF electronic wave functions. Our result on benzene radical cation agrees well with the experimental and theoretical values. Analysis by the vibronic coupling density reveals that the $e_{2g}(2)\theta$ and $e_{2g}(3)\theta$ vibrational modes including C–C stretching strongly couple with electron in the cation, while weakly couples with electron in the anion because of the reduction of electron density in the C–C bonds. In contrast, the $e_{2g}(4)\theta$ mode including C–H stretching moderately couples with electron in both cation and anion since the electron in the midpoint of C–C bonds has little coupling. This indicates that the magnitude of the vibronic coupling depends not only on the direction of the nuclear displacement but also on the phase pattern of the orbital. In other words, the difference on VCC between Bz^+ and Bz^- originates from the frontier electron density. This suggests that we can control a VCC by modifying its electronic structure. Studies along this line are in progress. The results will be published elsewhere.

ACKNOWLEDGMENTS

Numerical calculation was partly performed in the Supercomputer Laboratory of Kyoto University and Research Center for Computational Science, Okazaki, Japan.

[1] I. B. Bersuker, *The Jahn-Teller Effect and Vibronic Interactions in Modern Chemistry* (Plenum, New York, 1984).
[2] G. Fischer, *Vibronic Coupling: The Interaction Between the Electronic and Nuclear Motions* (Academic, London, 1984).
[3] I. B. Bersuker and V. Z. Polinger, *Vibronic Interaction in Molecules and Crystals* (Springer, Berlin, 1989).
[4] I. B. Bersuker, Chem. Rev. (Washington, D.C.) **101**, 1067 (2001).
[5] H. A. Jahn and E. Teller, Proc. R. Soc. London, Ser. A **161**, 220 (1937).
[6] P. M. Johnson, J. Chem. Phys. **117**, 9991 (2002).
[7] M. Döscher, H. Köppel, and P. G. Szalay, J. Chem. Phys. **117**, 2645 (2002).
[8] B. E. Applegate and T. A. Miller, J. Chem. Phys. **117**, 10654 (2002).
[9] C. D. Sherrill, M. S. Lee, and M. Head-Gordon, Chem. Phys. Lett. **302**, 425 (1999).
[10] T. Sato, K. Tokunaga, and K. Tanaka, J. Chem. Phys. **124**, 024314 (2006).
[11] D. W. Turner, Tetrahedron Lett. **8**, 3419 (1967).
[12] L. Åsbrink, E. Lindholm, and O. Edqvist, Chem. Phys. Lett. **5**, 609 (1970).
[13] M. Iwasaki, K. Toriyama, and K. Nunome, J. Chem. Soc., Chem. Commun. 320 (1983).
[14] A. D. Liehr, Z. Phys. Chem., Neue Folge **9**, 338 (1956).
[15] L. C. Snyder, J. Chem. Phys. **33**, 619 (1960).
[16] N. O. Lipari, C. B. Duke, and L. Pietronero, J. Chem. Phys. **65**, 1165 (1976).
[17] P. Pulay, G. Fogarasi, and J. E. Boggs, J. Chem. Phys. **74**, 3999 (1981).
[18] K. Raghavachari, R. C. Haddon, T. A. Miller, and V. E. Bondybey, J. Chem. Phys. **79**, 1387 (1983).
[19] L. Zhu and P. Johnson, J. Chem. Phys. **94**, 5769 (1991).
[20] W. B. Peatman, T. B. Borne, and E. W. Schlag, Chem. Phys. Lett. **3**, 492 (1969).
[21] D. P. Taylor, J. G. Goode, J. E. LeClaire, and P. M. Johnson, J. Chem. Phys. **103**, 6293 (1995).
[22] S. R. Long, J. T. Meek, and J. P. Reilly, J. Chem. Phys. **79**, 3206 (1983).
[23] H. Krause and H. J. Neusser, J. Chem. Phys. **97**, 5923 (1992).
[24] R. Lindner, K. Müller-Dethlefs, E. Wedum, K. Haber, and E. R. Grant, Science **271**, 1698 (1996).
[25] J. G. Goode, J. D. Hofstein, and P. M. Johnson, J. Chem. Phys. **107**, 1703 (1997).
[26] A. B. Burrill, Y. K. Chung, H. A. Mann, and P. M. Johnson, J. Chem. Phys. **120**, 8587 (2004).
[27] W. D. Hobey and A. D. McLachlan, J. Chem. Phys. **33**, 1695 (1960).
[28] A. L. Hinde, D. Poppinger, and L. Radom, J. Am. Chem. Soc. **100**, 4681 (1978).
[29] A. Klimkāns and S. Larsson, Chem. Phys. **189**, 25 (1994).
[30] M. T. Jones and T. C. Kuechler, J. Phys. Chem. **81**, 360 (1977).
[31] J. C. Moore, C. Thornton, W. B. Collier, and J. P. Devlin, J. Phys. Chem. **85**, 350 (1981).
[32] J. P. Devlin, J. S. McKennis, C. Thornton, and J. C. Moore, J. Phys. Chem. **86**, 2613 (1982).
[33] I. B. Bersuker, Kinet. Katal. **18**, 1268 (1977).
[34] I. B. Bersuker, Teor. Eksp. Khim. **14**, 3 (1978).

[35] I. B. Bersuker, Chem. Phys. **31**, 85 (1978).
[36] S. S. Stavrov, I. P. Decusar, and I. B. Bersuker, New J. Chem. **17**, 71 (1993).
[37] S. B. Piepho, J. Am. Chem. Soc. **110**, 6319 (1988).
[38] J. C. R. Faulhaber, D. Y. K. Ko, and P. R. Briddon, Phys. Rev. B **48**, 661 (1993).
[39] J. R. Letelier, Int. J. Mod. Phys. C **10**, 1177 (1999).
[40] M. J. Frisch, G. W. Trucks, H. B. Schlegel *et al.*, GAUSSIAN 03, Revision C.02, Wallingford, CT, 2004.
[41] Cambridge Analytic Derivative Package (CADPAC), Issue 6.5, Cambridge, UK, 2001.
[42] T. Kato and T. Yamabe, J. Chem. Phys. **115**, 8592 (2001).